EMBRY-RIDDLE
Aeronautical University
SCHOLARLY COMMONS

Publications

7-1-2022

Climatology of Deep O+ Dropouts in the Night-Time F-Region in Solar Minimum Measured by a Langmuir Probe Onboard the International Space Station

Shantanab Debchoudhury
Embry-Riddle Aeronautical University, debchous@erau.edu

Aroh Barjatya
Embry-Riddle Aeronautical University, barjatya@erau.edu

Joseh I. Minow
NASA Marshall Space Flight Center

Victoria N. Coffey
NASA Marshall Space Flight Center

Linda N. Parker
Space Weather Solutions

Follow this and additional works at: https://commons.erau.edu/publication

 Part of the Instrumentation Commons

Scholarly Commons Citation

Debchoudhury, S., Barjatya, A., Minow, J. I., Coffey, V. N., & Parker, L. N. (2022). Climatology of deep O+ dropouts in the night-time F-region in solar minimum measured by a Langmuir Probe onboard the International Space Station. Journal of Geophysical Research: Space Physics, 127, e2022JA030446. https://doi.org/10.1029/2022JA030446

This Article is brought to you for free and open access by Scholarly Commons. It has been accepted for inclusion in Publications by an authorized administrator of Scholarly Commons. For more information, please contact commons@erau.edu.

Check for updates

Climatology of deep O+ dropouts in the night-time F-region in solar minimum measured by a Langmuir Probe onboard the International Space Station

Shantanab Debchoudhury[1], Aroh Barjatya[1], Joseph I. Minow[2], Victoria N. Coffey[2], Linda N. Parker[3]

[1]Embry Riddle Aeronautical University, Daytona Beach, FL
[2]NASA, Marshall Space Flight Center, Huntsville, AL
[3]Space Weather Solutions, Huntsville, AL

Key Points:

- O^+ percentages often drop below 80% at ISS altitudes during solar minimum
- The dropouts in O^+ abundance are common in post-midnight sector in winter hemisphere
- The climatology of the dropouts is governed by neutral wind variations and lowered O^+/H^+ transition height.

Corresponding author: Shantanab Debchoudhury, debchous@erau.edu

This article has been accepted for publication and undergone full peer review but has not been through the copyediting, typesetting, pagination and proofreading process, which may lead to differences between this version and the Version of Record. Please cite this article as doi: 10.1029/2022JA030446.

This article is protected by copyright. All rights reserved.

Accepted Article

Accepted Article

Abstract

The Floating Potential Measurement Unit (FPMU) onboard the International Space Station includes a Wide sweeping Langmuir Probe (WLP) that has been operating in the F-region of the ionosphere at ∼400 km since 2006. While traditional Langmuir probe estimates include critical plasma parameters like electron density and temperature, we have also extracted the O^+ percentage from the total ion constituents. This O^+ composition dataset from the recent minimum in the Solar Cycle 24 reveals orbits with dropouts in O^+ to below 80% of the total background ion density at ISS orbital altitudes. The observed O^+ percentages during these dropouts are much lower than the values predicted by the International Reference Ionosphere 2016 (IRI2016) empirical model. In this paper, we present the climatology of these O^+ dropouts with their dependency on season, local time and geographical location. The results show that the lowered O^+ percentages are more significant in the winter hemispheres and are routinely observed for orbits in the pre-sunrise periods. The patterns in O^+ dropouts can be explained in part from the lowering of the O^+/H^+ transition height during solar minimum along with patterns in neutral wind variation.

Plain Language Summary

The plasma environment experienced by the International Space Station (ISS) is of key importance to the space physics community. A suite of instruments on the ISS has been operating since 2006 that consist of a spherical Langmuir probe, called the WLP, which is a sensor that periodically collects information about the density and energy of the ambient electrons. Recently we presented a technique to also infer the composition of O^+ ions relative to the total ion density which is an important parameter in understanding the interaction between the terrestrial atmosphere with the exosphere. Results from the most recent period of solar minimum reveal dropouts in O^+ densities compared to predictions from empirical models. We show global climatology plots from 2018 and 2019 and observe that these large dropouts in O^+ are more prevalent in the post-midnight region of the winter hemisphere. Past studies have discussed increased presence of lighter H^+ ions at higher orbital altitudes, but the fact that O^+ dropouts are observed even at ISS altitudes is striking and one of the prominent features of solar minimum.

1 Introduction

The Wide sweeping Langmuir probe (WLP) is a gold-coated spherical Langmuir Probe and one of four instruments that constitutes the Floating Potential Measurement Unit (FPMU) (Barjatya et al., 2009) hosted on the International Space Station (ISS). While the primary objective of the FPMU is to monitor the charging of the ISS (Wright et al., 2008; Koontz et al., 2020), the data products from the instruments can be useful for understanding the behavior and dynamics of the F-region ionosphere at a nominal altitude of ∼ 400km. With the orbital inclination of the ISS at 51.6°, the FPMU data products cover low- and mid-latitudes and have been recorded since 2006. In particular, the WLP is swept over a wide range of voltages, from -20 V to 80 V, with respect to the chassis ground, and the resulting collected current-voltage (I-V) profile can be analyzed to estimate the ambient electron density and temperature at a cadence of 1 Hz along the ISS orbit. Owing to this wide sweep that goes deep in the ion saturation region, it is possible to fit for multiple ion species. Recently Debchoudhury et al. (2021) re-analyzed the WLP data, ranging from 2006 to 2020, to extract the relative split of the heavier O^+ to lighter H^+ ions in the topside ionosphere. The resulting composition data showed rapid drops of O^+ percentage in a number of orbits during the most recent solar minimum of Solar Cycle 24 in the years 2018 and 2019, which we now explore further in this paper.

This article is protected by copyright. All rights reserved.

Accepted Article

A number of observations in the past, both ground-based and in-situ, have been used to understand the ionospheric F-region composition in solar minimum conditions. Incoherent scatter radar (ISR) observations over Arecibo showed that there is a discernible impact on the ionosphere near the O^+/H^+ transition region resulting from the large difference in masses and velocities (Hagen & Hsu, 1974; Vickrey et al., 1976, 1979b, 1979a) which describe the coupling between the protonosphere and the ionosphere. Similarly, Evans and Holt (1971, 1978) used data from the Millstone-Hill ISR to study the coupling between the ionosphere and the plasmasphere and its impact on the O^+ fluxes with season and solar activity. The local time and seasonal dependence on the two ion fluxes were explored theoretically by Bailey et al. (1977, 1982, 1987). They found that interhemispheric transport can be significant especially at low latitudes where the net flux tube content in the protonosphere is much smaller compared to the ionosphere.

In-situ ion composition data from the topside ionosphere are, most often, measured by ion mass spectrometers and retarding potential analyzers (RPAs) on a satellite platform. Breig et al. (1992) presented data from the RPA and the magnetic and Bennett ion mass spectrometers (MIMS and BIMS resepctively) onboard the Atmospheric Explorer C (AE-C) mission to demonstrate strong ion flows and decreases in O^+/H^+ ratio in the winter hemisphere at 500 km. The composition data from the BIMS and MIMS onboard the AE-C and AE-E satellites and BIMS data from the Intercosmos 24 (IK-24) satellite are the bases of the TTS03 empirical model by Třísková et al. (2003). This model was improved by Truhlík et al. (2015)to the TBT15 model, which serves as the default topside composition setting for the International Reference Ionosphere 2016 (IRI2016) empirical model (Bilitza et al., 2017). Truhlík et al. (2004) validated the IK24 BIMS data to an RPA operating in the planar trap mode on the same satellite for solar maximum and demonstrated that the upper transition height was significantly raised in daytime and high solar activity. Heelis et al. (2009) and Klenzing et al. (2011) used RPA data from the C/NOFS satellite (de La Beaujardière et al., 2004) in a low-inclination orbit to study the variation in the O^+/H^+ transition height during the prolonged deep minimum of Solar Cycle 23. Very recently, Huba et al. (2021) reported instances of dropout in O^+ densities from measurements made by the Ion Velocity Meter (IVM) instrument from the Ionospheric Connection Explorer (ICON) satellite at an altitude of 600 km and an orbital inclination of 27°. The authors argue that the lowered O^+/H^+ transition height from the prolonged downward $\mathbf{E}\times\mathbf{B}$ drift in the pre-midnight sector contribute to the decrease in topside O^+ densities during solar minimum as indicated by previous studies performed by Hysell et al. (2009) and Klenzing et al. (2011). The downward $\mathbf{E}\times\mathbf{B}$ drift is the mechanism that directly explains the lowering of the O^+/H^+ transition height for the equatorial ionosphere.

In this paper, we present the spatial and temporal distribution of the O^+ observations recorded over the most recent minimum of Solar Cycle 24. To the best of our knowledge, the data presented here serve as the largest dataset of the ion composition near 400 km spanning the minimum of Solar Cycle 24 and the only one derived from Langmuir probe measurements. Additionally with the ISS in a mid-inclination orbit, the resulting data covers all longitude sectors within a geodetic latitude range of $\sim \pm 52°$ allowing us to investigate broad seasonal and solar activity impact over the mid- and low-latitudes. The rest of the paper is arranged as follows: in the succeeding section, we present the nature of these O^+ dropouts and their seasonal, local time and geographic dependencies. We follow this with discussions on the features observed in the climatology of the O^+ dropouts, before concluding with remarks on the contributions of the measurements to the ionospheric and space physics community.

This article is protected by copyright. All rights reserved.

Accepted Article

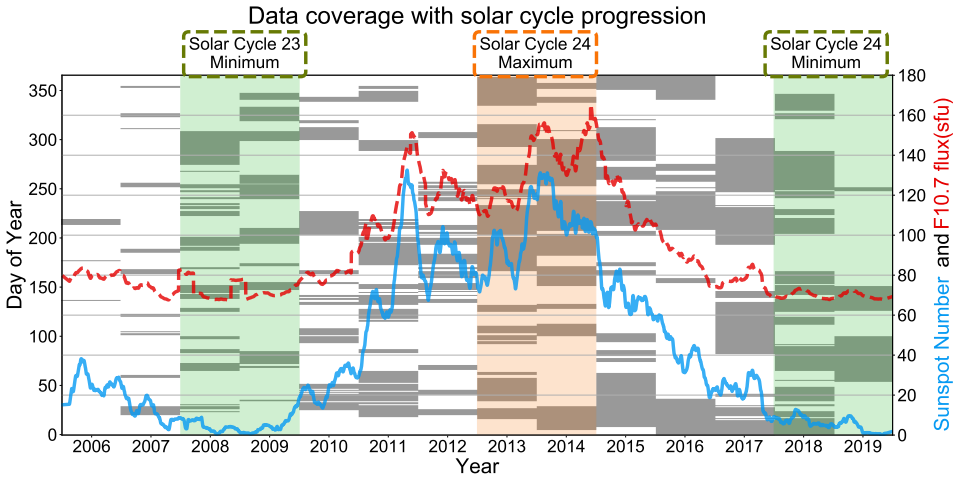

Figure 1. The figure shows operational status of the FPMU first unit over its nearly 13 year lifetime. The panel to the left shows the days of the year when FPMU was operational, while the panel to the right charts the variation of the sunspot number (blue) and the solar F10.7 flux (red). The green shadowed regions highlight the solar minimum, while the red shadowed region highlights solar maximum.

2 Data Presentation

2.1 Observations

Figure 1 shows the progression of the solar cycle during the lifetime of this FPMU from 2006 through 2020. This first one was replaced by a second FPMU that became operational in 2021. Thus, data presented here are not from the recently installed FPMU. The days when FPMU was operational are shown as shadowed blocks as a function of the day of the year shown on the left y-axis. The panel to the right records the sunspot number and the F10.7 solar flux in blue and red respectively, both of which are frequently used to quantify the level of solar activity. Each of these solar indices has been smoothed using a 91-day moving average filter. Shadowed sections in green show the last two solar minima of Solar Cycles 23 and 24 when both the solar flux and sunspot numbers were lowest. As can be seen in Figure 1, the two minima are very much comparable with the median F10.7 fluxes being ∼69 solar flux units (sfu) for each of the two solar cycle phases. The median sunspot number was also 0 for these minima of the last two solar cycles.

For the purposes of the paper, we focus on the years 2018 and 2019, when the solar activity was low in the declining phase of Solar Cycle 24. It is important to note that while the FPMU has been operational since 2006, the data collection is not continuous but rather on a campaign basis. The bulk of this data is in Solar Cycle 24 which makes the most recent minimum a more complete time segment to study the F-region ionospheric behavior.

The data from the FPMU over the years 2018 and 2019 show that the recorded plasma densities were lower, and the measured electron temperatures were higher compared to the predictions by the IRI2016 model. The algorithm used to derive these parameters has been discussed in detail by Debchoudhury et al. (2021). In the same paper, the authors detail the process of extracting ion composition information from the ion-saturation region of the WLP. The most abundant ion at F-region altitudes is the singly-charged O^+ ion that is generally significantly higher in composition than heavier molecular ions that are typically present at lower altitudes and lighter H^+ and He^+ ions which are more

This article is protected by copyright. All rights reserved.

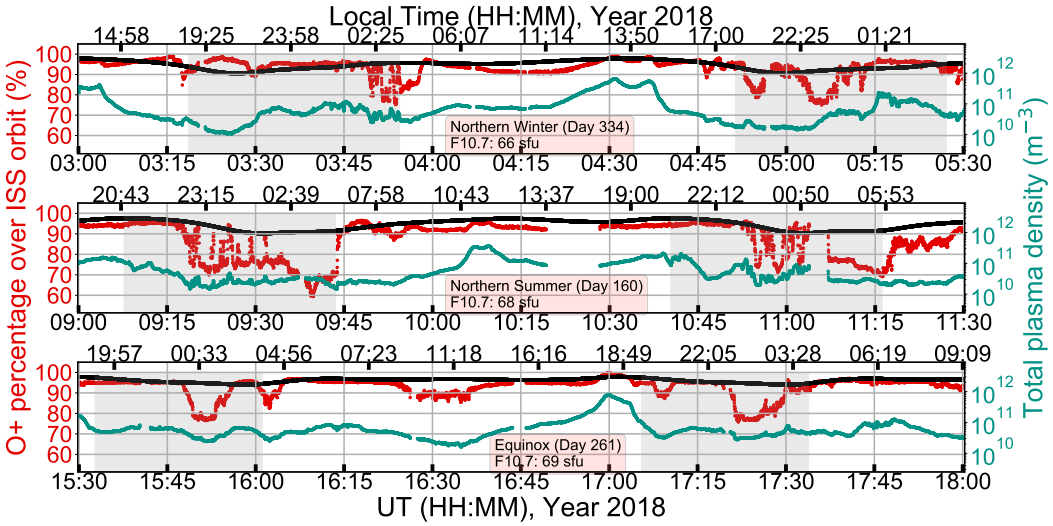

Figure 2. The panels show O^+ percentage composition measured by the WLP (red, left axis) and predicted by the IRI (black, left axis). Also shown for reference is the quasineutral plasma density obtained from the WLP (green, right axis). From top to bottom, the three panels present data in the solar minimum of 2018 over three days in the seasons which are Northern Winter, Northern Summer and Equinox respectively. For each panel, the top axis describes the local time and the bottom axis shows the universal time, while greyed out regions show times when the sun is fully eclipsed from the ISS.

important at higher altitudes above the O^+/H^+ transition altitude. However, the FPMU 2018-2019 orbit-track O^+ abundance data product revealed sharp drops in O^+ composition down to 80% of the total density and lower for some orbits.

Figure 2 shows a few orbits from three such days in 2018 when these dropouts were detected. Each panel in Figure 2 represent a day in three different seasons when both the solar and geomagnetic activities were low. The variation in the O^+ percentage along the ISS orbit is shown in red as measured by the WLP, while the IRI prediction is described in black. For all the figures in the paper, the IRI predictions are computed using the pyglow python wrapper for IRI2016 where the default topside composition is from the TBT15 model (Truhlík et al., 2015). The universal time (UT) and the local time along the ISS path are shown on the bottom and top axes respectively, while the greyed out regions demarcate eclipse conditions (zero solar intensity) as seen by the ISS at F-region altitudes. In addition, we show the total quasineutral plasma density in green along the right axis for each panel. For all the three cases presented, O^+ percentages recorded over the night-time F-region were much lower than IRI predictions and show instances when the relative presence of O^+ number density drops below 80% of the background ions. For the orbits presented the total density profile did not present evidence of dawn density depletions like the ones reported in solar minimum by de La Beaujardière et al. (2009) and Gentile et al. (2011). Thus, the dropouts in O^+ densities are not indicative of the presence or absence of dawn density depletions as reported from the C/NOFS and DMSP satellites. These O^+ dropouts at F-region altitudes were briefly discussed in Debchoudhury et al. (2021), but their occurrence is investigated in a greater detail in this paper. In particular, we attempt to investigate the broad climatology of these O^+ dropouts over the days for which FPMU was operational in the minimum of Solar Cycle 24 spanning the years 2018 and 2019.

This article is protected by copyright. All rights reserved.

Accepted Article

Accepted Article

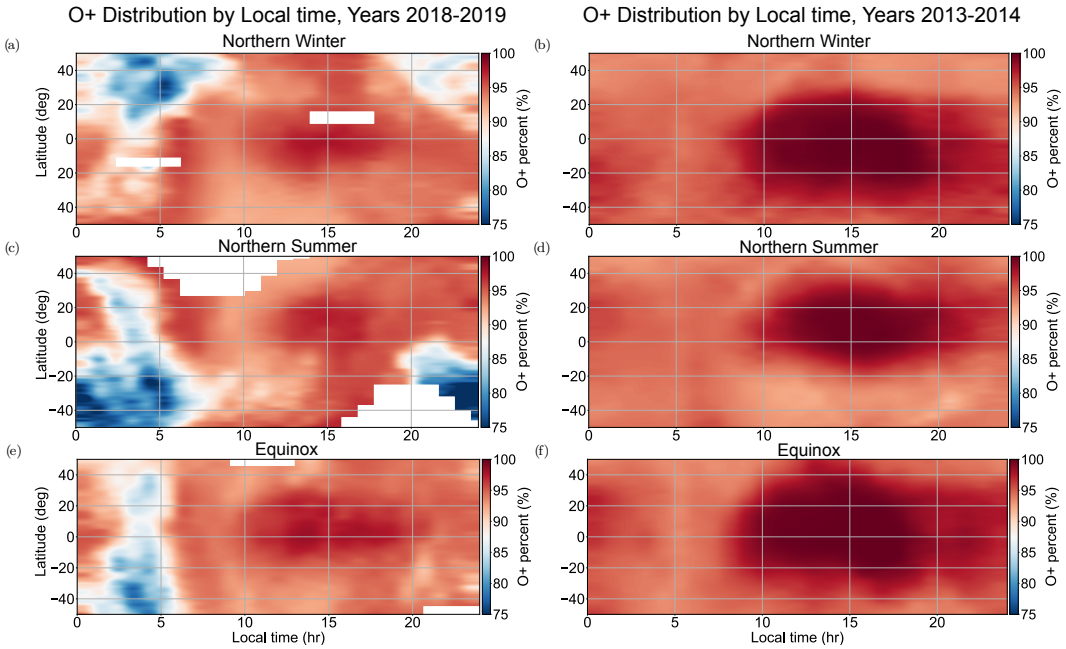

Figure 3. O^+ percentages measured by the WLP instrument as a function of geodetic latitude versus local time sector are shown in each panel. Panels (a), (c) and (e) describe the variation over the minimum of Solar Cycle 24 (1/2018 - 12/2019), while panels (b), (d) and (f) show the variation over two years of solar maximum (1/2013 - 12/2014) in the same solar cycle. In addition, the three rows of panels describe the seasonal variation of the O^+ variability, with panels (a) and (b) showing Northern Winter conditions, (c) and (d) describing the Northern summer season, and (e) and (f) indicating equinoctial conditions.

2.2 Latitude versus Local Time

The dependence of the O^+ percentage composition on season is studied by classifying the day of the year (DOY) into 3 broad seasonal categories:

1. Northern Winter: DOY 1 (Jan 1) - DOY 60 (Mar 1), DOY 305 (Nov 1) - DOY 365 (Dec 31)
2. Northern Summer: DOY 121 (May 1) - DOY 243 (Aug 31)
3. Equinox: DOY 61 (Mar 2) - DOY 120 (Apr 30), DOY 244 (Sep 1) - DOY 304 (Oct 31)

For each day in each of the seasons in 2018 and 2019, the measured O^+ percentage is binned into a 1° latitude sector for every 1 hour of local time ranging from 0 to 24 hours. The mean O^+ percentage is thus obtained by averaging the aggregated oxygen ion composition values over each bin and smoothed using a Gaussian filter (refer to matplotlib package in python for details). Gaps in data have been interpolated unless several successive pixels are missing (not sufficient data), which we present as blocks of white spots in the images. The resulting numbers are shown as colorplots in Figure 3. Panels (a), (c) and (e) show the aggregated O^+ distribution in the years of solar minimum 2018 and 2019 for the three seasons - Northern Winter, Northern Summer and Equinox respectively. For comparison purposes, the panels (b), (d) and (f) describe the same for the years of solar maximum ranging from 2013 and 2014. For each panel, the colorbars indicate the O^+ percent composition levels from 75% (more blue) to 100% (more red).

This article is protected by copyright. All rights reserved.

Accepted Article

As is evident in Figure 3, dropouts in O^+ abundance were frequently recorded by the FPMU in the night-time F-region ionosphere during solar minimum, while these dropouts were absent in solar maximum. The O^+ dropouts are more prevalent in the post midnight ionosphere for all three seasons, and more intense in the winter hemispheres. In the Northern Summer case, some of the O^+ dropouts were also recorded in the post-sunset pre-midnight time period, which are mostly congregated in the southern hemisphere in accordance with the general tendency of the dropouts to be abundant during winter. For both the solar minimum and solar maximum years, the highest O^+ percentages were measured in the afternoon sector with the maximum number much closer to 100% in solar maximum compared to solar minimum.

2.3 Climatology of post-midnight O^+ dropouts

We focus on the post-midnight dropouts in O^+ densities and investigate possible patterns in their geographical distribution over the three seasons. Such climatological descriptions of depletions have been reported from DMSP and CNOFS topside ionosphere density records (de La Beaujardière et al., 2009; Gentile et al., 2011) but these studies did not resolve the O^+ composition. For this study we focus only on the local times of 00-05 LT for the solar minimum years of 2018 and 2019. Similar to the procedure outlined for Figure 3, we accumulate the O^+ composition data into $1^\circ \times 1^\circ$ latitude-longitude bins for every season. The data were then smoothed using an uniform filter with a sliding window of $5^\circ \times 10^\circ$ in the latitude and longitude direction respectively. The resulting average distribution of the O^+ abundance is plotted on a map for every season and shown for the three panels in Figure 4. Panel (a) represents the Northern Winter case, panel (b) describes the Northern Summer case, while panel (c) indicates the behavior over equinox. Data from the white patch in the Indian sector during the Northern Winter and Northern Summer plot has been intentionally removed since the data over this sector was not available over a significant amount of locations to perform a realistic smoothing operation.

Similar to Figure 3, in Figure 4, we find that in non-equinoctial conditions, the bulk of the lower O^+ densities were in the winter hemisphere. So, for the Northern Winter case, the nighttime post-midnight O^+ dropouts are present predominantly in the Northern Hemisphere, while for the Northern Summer, the lowest O^+ percentages are seen in the Southern Hemisphere. For equinox, low O^+ abundance are seen in both hemispheres on either side of the magnetic equator, and are on an average much less severe than the low percentages seen in summer and winter. The general climatology of the O^+ variation agrees with the IRI predictions as seen from the corresponding panel to the right in Figure 4. However, as is also seen in Figure 2, the empirical IRI model does not predict any of the deep O^+ dropouts observed by the WLP and the average IRI magnitude of the low O^+ percentage in the winter hemisphere is higher than that observed by the WLP. Thus, the colorbar range for the IRI plots in Figure 4 are intentionally made different with a much higher percent value for the lower limit to reveal the hemispherical differences in predicted O^+ abundance. The patterns demonstrated by Figure 4 also reveal a number of significant differences between the WLP measurements and the IRI predictions which we highlight below:

1. In the the Northern hemisphere during the Northern Winter season, low O^+ percentages below 80% were observed in all longitude sectors, except for the region between 60°W - 0°, where the O^+ percentages were higher.
2. Similar to the IRI prediction, the observed O^+ densities are deeper for the southern winter than the Northern Winter. However, in the the Southern winter, deep dropouts in O^+ densities were seen over the South Atlantic ocean which had the deepest seen O^+ dropouts across all three seasons.

This article is protected by copyright. All rights reserved.

Accepted Article

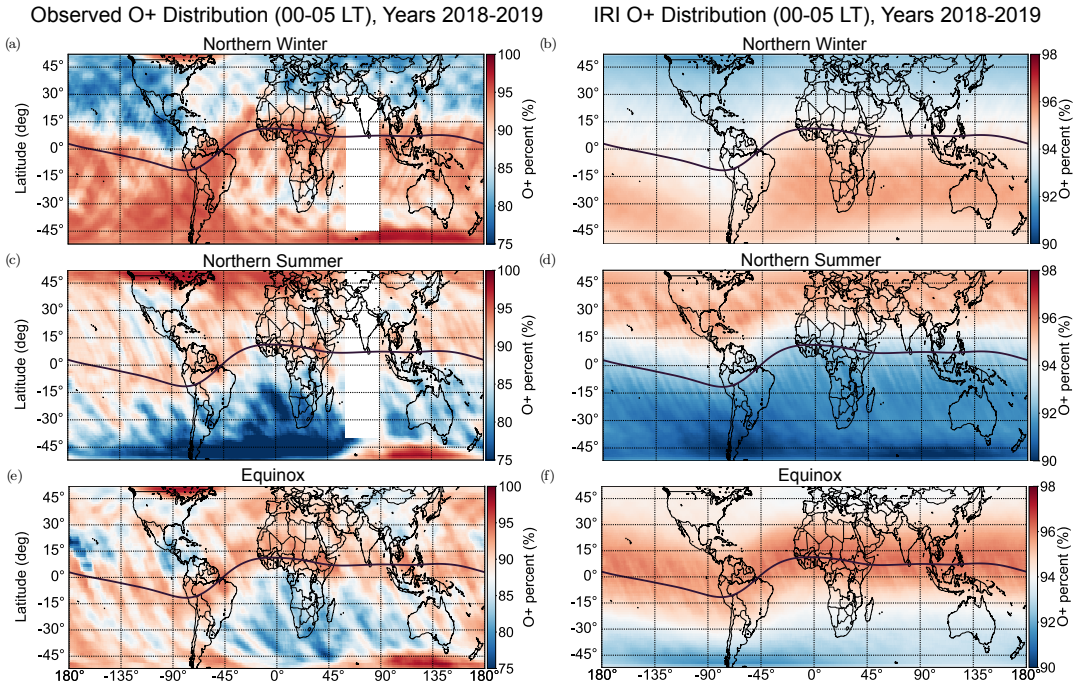

Figure 4. Figure shows the spatial distribution of the O^+ abundance measured by the WLP over Northern Winter (panel a), Northern Summer (panel c) and equinox (panel e) in the years 2018 and 2019. The corresponding IRI predictions are shown in panles (b), (d) and (f), respectively. The colors in the figure conform to the colorbar shown to the right of each panel. The magnetic equator is shown with a black line for reference in each of the plots.

3. For the same season (Northern Summer), the O^+ abundance in the summer hemisphere over the higher mid-latitudes (40°S and higher) in the longitude sector between 60°E - 0° is higher than neighboring regions.

3 Discussions

The relative concentration of the O^+ and H^+ ion in the F-region ionosphere at 400 km is affected by a number of factors. The primary chemical equation that determines the ionospheric composition is the charge-exchange process (Rishbeth & Garriott, 1969):

$$O^+ + H \rightleftharpoons O + H^+. \tag{1}$$

The resulting O^+ densities would hence depend directly on the neutral number density ratio $\frac{[O]}{[H]}$. Haaser et al. (2010) presented evidence that the cold thermosphere near 400 km in pre-sunrise hours during the minimum of 2008-2009 was predominantly composed of lighter hydrogen and helium which indicates that the fractional oxygen to hydrogen ratio $\frac{[O]}{[H]}$ may be depleted which would reduce the O^+ percentage. Similarly Kotov et al. (2015) showed calculations from a physical model to argue that redistribution of neutral hydrogen during prolonged periods of diminished solar activity can increase the neutral hydrogen over mid-latitude topside ionosphere and result in O^+ percentage reduction which was subsequently observed over Ukraine in the equinox periods of the minimum of Solar Cycle 23. The reduced O^+ percentages from the FPMU WLP dataset in Figures 3 and 4 indicate that this is a possible explanation for the deep O^+ dropouts in the post-midnight F-region ionosphere during solar minimum.

This article is protected by copyright. All rights reserved.

Accepted Article

The O^+/H^+ transition height is also a key factor in regulating the composition in the F-region ionosphere. Huba et al. (2021) presented model simulations to show that the O^+/H^+ transition height was lowered to 500 km during the night in December 2019 when ICON observed dropouts of O^+ densities at 600 km. Since O^+ densities decrease and H^+ densities increase rapidly as the altitude approaches the O^+/H^+ transition height (Figure 4, Huba et al. (2021)), a lowering of the O^+/H^+ transition height to a heights close to the ISS orbit would entail significant reduction in the O^+ percentage composition. Heelis et al. (2009) observed from in-situ C/NOFS satellite data that the transition altitude at night in the low-latitudes fell to 450 km during the minimum of Solar Cycle 23. Measurements from Arecibo incoherent scatter radar during equinox of the same solar minimum, presented by Aponte et al. (2013), agreed with these findings where the authors show that the transition height was lowest in the pre-sunrise sector and much lower than IRI predictions. Since the ISS is maintained in a nearly circular orbit, it is impossible to determine the transition height as it had been done with C/NOFS by Heelis et al. (2009). However, given that the depth of the minima of Solar Cycles 23 and 24 are comparable, as seen in Figure 1, it is not unreasonable to assume that the transition height could have been lowered to similar low altitudes, close to the ISS, for a number of days during the post midnight period during 2018 and 2019. This, in turn, can explain the O^+ density dropouts that we observe in the WLP data. Interestingly, similar to the observations reported by Huba et al. (2021), instances of equatorial plasma bubbles (EPBs) and nighttime irregularities were also encountered by the ISS for a number of orbits. The corresponding O^+ densities within these irregularities were structured showing some dropouts; however, the occurrence conditions and level of these O^+ dropouts inside EPBs have not been studied yet and will be subject of a future study.

Neutral winds also play a key role in determining the longitudinal variations of the plasma composition and modulating the effect of the lowered transition height. This was demonstrated by West and Heelis (1996) in a study of the 1993 solar minimum using DMSP data at 700 km. Similar arguments presented by the authors also apply to the geographical distribution of O^+ percentages seen in Figure 4. To demonstrate this we present in Figure 5, the average meridional and zonal winds as obtained from the Horizontal Wind Model, Drob et al. (2015) (HWM 14), for the same period of time in which the WLP collected data in the post-midnight sector (00-05 LT). These are arranged for the different seasons as in Figures 3 and 4. Also shown are the dip and declination contours of the geomagnetic field in panels (g) and (h), which aid the logic of the following discussion.

The direction of plasma flow at the F-region altitudes, in response to a neutral wind, is most affected by the component of the neutral wind parallel to the magnetic field (Rishbeth & Garriott, 1969). Of particular importance, in this context, is the role in moving plasma upwards or downwards in altitude since the lifted or lowered ionosphere can change the composition measured at a certain altitude. Coupled with commonly observed physical processes observed in solar minimum such as the lowering of the O^+/H^+ transition altitude (Heelis et al., 2009) and the interhemispheric field-aligned H^+ flux from the summer to the winter hemisphere (Bailey et al., 1987), a significant downward plasma motion can reduce the relative O^+ composition at ISS altitudes.

When the dip angle is non-zero, the contribution of the neutral winds can be significant in relation to the vertical motion of the plasma. In general, for magnetic field lines with an eastward declination, an eastward (positive) zonal wind will move plasma downwards in the Northern latitudes while a westward zonal wind will move plasma up along the field line. For low and mid geomagnetic latitudes, a northward (positive) meridional wind moves plasma down a field line in the magnetic north latitudes since the dip angle is downward (positive) while the reverse is true for southern latitudes. This explains the relatively higher O^+ percentage in Northern Winter over the mid-latitude Atlantic sector between 60°W - 0° in Figure 4a. Here the wind is southward (Figure 5a), primarily eastward (Figure 5b), both of which drives plasma up the westward field line

This article is protected by copyright. All rights reserved.

Accepted Article

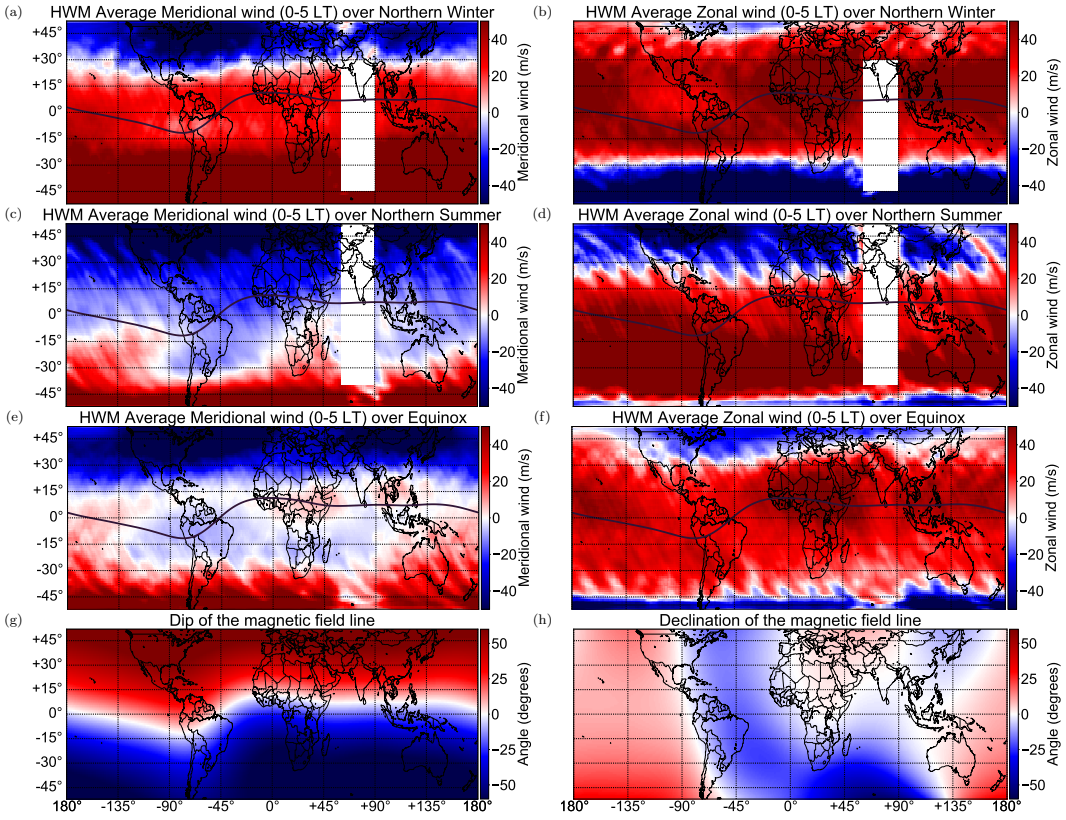

Figure 5. Figure shows the meridional (panels a,c,e) and zonal winds (panels b,d,f) as predicted by HWM at the same time when FPMU recorded data in the years 2018 and 2019. The wind patterns are shown for the three seasons - Northern Winter (panels a,b), Northern Summer (panels c,d) and equinox (e,f). The dip and declination of the magnetic field lines at ISS altitudes are also shown in panels g and h respectively.

(Figure 5h) and account for the increased O^+ relative to the rest of the Northern Hemisphere. For high geomagnetic latitudes when the dip angle is very high, meridional winds do not have a big impact in moving plasma up or down in altitude. At these latitudes, if the declination of the magnetic field is significant, zonal winds play a crucial role instead. This effect is reflected in the higher O^+ percentage in the southern high latitude region of Figure 4c which matches with the pattern of the westward zonal wind (Figure 5d). This is a region where field lines are almost vertical and to the west (Figure 5h) in the longitude region between 60°E - 120°E and the upward moving plasma lifts the F-peak higher.

In other places, the effect of the neutral wind is much more complicated and relies on accurate measurements of winds. For example, the deep O^+ dropout in the South Atlantic sector in Northern Summer and moderately in the equinox seasons cannot be explained solely by the HWM horizontal winds. Here the negative declination (Figure 5h) and eastward zonal wind (Figure 5d) would imply increased H^+ due to favorable conditions of plasma velocities down the upward pointing field line, but the northward meridional winds show a tendency to counter this effect. Figure 5c show that a region of separation exists when meridional winds turn northward in Southern winter, which if more southwards, could possibly explain the deep O^+ density dropouts. A vertical wind, which is generally assumed to be negligibly small compared to the horizontal winds, could also be significant at these latitudes. Finally, precise calculations of the interhemispheric flux

This article is protected by copyright. All rights reserved.

Accepted Article

using observations can possibly provide some explanation for the behavior in these regions which can only be monitored using satellites. In equinoctial conditions, the meridional wind has much less of an effect in producing asymmetrical composition responses in the different hemispheres, since for moderate dip angles of the field-line, the values of the meridional wind are smaller (Figure 5e). Instead the zonal wind patterns in Figure 5f play some role in the different responses for different geomagnetic declinations, as discussed by West and Heelis (1996).

4 Conclusions

We present observations of O^+ percentage composition measured by the WLP instrument from the FPMU suite onboard the ISS. Data from the most recent solar minimum from 2018 and 2019 reveal frequently seen dropouts in the relative O^+ percentage which was not observed in solar maximum. The O^+ percentages often dropped below 80%, and are seen in the post-midnight sector of the winter hemisphere. Seasonal asymmetries are also seen with the southern winter recording more intense O^+ dropouts, concentrated over the South Atlantic sector, versus the Northern Winter hemisphere. These drops in O^+ percentage are not captured by the empirical IRI model and the data suggest that these dropouts occur frequently depending on season and local time. Several aspects of the climatological features can be explained through global wind patterns over varying geomagnetic regions. However, future studies need to be performed with modeling and observations, particularly of the neutral winds and the interhemispheric flux, to augment the observations and understand the physical processes that are responsible for their occurrence.

Acknowledgments

S. Debchoudhury was supported for this work through NASA contract TI-19-01434. The authors would like to acknowledge a number of data sources used for the project. These include open-source python software packages pyglow for IRI (`https://github.com/timduly4/pyglow`) and LMfit version 0.9.14 (`https://lmfit.github.io/lmfit-py/`) for non-linear curve fitting. The re-processed FPMU data set including the recently derived O+ percentages will replace the existing dataset hosted at the NASA Space Physics Data Facility at `https://cdaweb.gsfc.nasa.gov/pub/data/international_space_station_iss/sp_fpmu/`. The authors would also like to thank all the FPMU team members at JSC and MSFC for their efforts. In addition the data generated for this article will be made available for open access at `https://doi.org/10.5281/zenodo.6245938`.

References

Aponte, N., Brum, C. G., Sulzer, M. P., & González, S. A. (2013). Measurements of the O+ to H+ transition height and ion temperatures in the lower topside ionosphere over arecibo for equinox conditions during the 2008–2009 extreme solar minimum. *Journal of Geophysical Research: Space Physics*, *118*(7), 4465–4470.

Bailey, G., Moffett, R., & Murphy, J. (1977). Relative flow of H+ and O+ ions in the topside ionosphere at mid-latitudes. *Planetary and Space Science*, *25*(10), 967–972.

Bailey, G., Simmons, P., & Moffett, R. (1987). Topside and interhemispheric ion flows in the mid-latitude plasmasphere. *Journal of atmospheric and terrestrial physics*, *49*(6), 503–519.

Bailey, G., Vickrey, J., & Swartz, W. (1982). The topside ionosphere above arecibo during summer at sunspot minimum and the influence of an interhemispheric flow of thermal protons. *Journal of Geophysical Research: Space Physics*, *87*(A9), 7557–7567.

This article is protected by copyright. All rights reserved.

Barjatya, A., Swenson, C. M., Thompson, D. C., & Jr., K. H. W. (2009). Invited article: Data analysis of the floating potential measurement unit aboard the international space station. *Review of Scientific Instruments*, *80, 041301*. doi: 10.1063/1.3116085

Bilitza, D., Altadill, D., Truhlik, V., Shubin, V., Galkin, I., Reinisch, B., & Huang, X. (2017). International reference ionosphere 2016: From ionospheric climate to real-time weather predictions. *Space Weather*, *15*(2), 418–429.

Breig, E., Sanatani, S., & Hanson, W. (1992). Spatial variations of the [H+]/[O+] ion concentration ratio in the topside f region: Observational evidence for H+ ion flows. *Journal of Geophysical Research: Space Physics*, *97*(A5), 6299–6313.

Debchoudhury, S., Barjatya, A., Minow, J. I., Coffey, V. N., & Chandler, M. O. (2021). Observations and validation of plasma density, temperature, and O+ abundance from a langmuir probe onboard the international space station. *Journal of Geophysical Research: Space Physics*, *126*(10), e2021JA029393.

de La Beaujardière, O., et al. (2004). C/NOFS: A mission to forecast scintillations. *Journal of Atmospheric and Solar-Terrestrial Physics*, *66*(17), 1573–1591.

de La Beaujardière, O., Retterer, J. M., Pfaff, R. F., Roddy, P. A., Roth, C., Burke, W. J., ... others (2009). C/NOFS observations of deep plasma depletions at dawn. *Geophysical Research Letters*, *36*(18).

Drob, D. P., Emmert, J. T., Meriwether, J. W., Makela, J. J., Doornbos, E., Conde, M., ... others (2015). An update to the horizontal wind model (hwm): The quiet time thermosphere. *Earth and Space Science*, *2*(7), 301–319.

Evans, J., & Holt, J. (1971). Observations of f-region vertical velocities at millstone hill 3. determination of altitude distribution of H+. *Radio Science*, *6*(10), 855–861.

Evans, J., & Holt, J. (1978). Nighttime proton fluxes at millstone hill. *Planetary and Space Science*, *26*(8), 727–744.

Gentile, L., Burke, W., Roddy, P., Retterer, J., & Tsunoda, R. (2011). Climatology of plasma density depletions observed by dmsp in the dawn sector. *Journal of Geophysical Research: Space Physics*, *116*(A3).

Haaser, R., Earle, G., Heelis, R., Coley, W., & Klenzing, J. (2010). Low-latitude measurements of neutral thermospheric helium dominance near 400 km during extreme solar minimum. *Journal of Geophysical Research: Space Physics*, *115*(A11).

Hagen, J. B., & Hsu, P. Y.-S. (1974). The structure of the protonosphere above arecibo. *Journal of Geophysical Research*, *79*(28), 4269–4275.

Heelis, R., Coley, W., Burrell, A., Hairston, M., Earle, G., Perdue, M., ... Lippincott, C. (2009). Behavior of the O+/H+ transition height during the extreme solar minimum of 2008. *Geophysical Research Letters*, *36*(18).

Huba, J., Heelis, R., & Maute, A. (2021). Large-scale O+ depletions observed by icon in the post-midnight topside ionosphere: Data/model comparison. *Geophysical Research Letters*, *48*(7), e2020GL092061.

Hysell, D., Nossa, E., Larsen, M., Munro, J., Sulzer, M., & González, S. (2009). Sporadic e layer observations over arecibo using coherent and incoherent scatter radar: Assessing dynamic stability in the lower thermosphere. *Journal of Geophysical Research: Space Physics*, *114*(A12).

Klenzing, J., Simões, F., Ivanov, S., Heelis, R., Bilitza, D., Pfaff, R., & Rowland, D. (2011). Topside equatorial ionospheric density and composition during and after extreme solar minimum. *Journal of Geophysical Research: Space Physics*, *116*(A12).

Koontz, S., Castillo, T., Hartman, W., Schmidl, W., Haught, M., Duncan, G., ... Vera, J. (2020). International space station spacecraft charging hazards: Hazard identification, management, and control methodologies, with possible applications to human spaceflight beyond leo. *Journal of Space Safety*

This article is protected by copyright. All rights reserved.

Accepted Article

Engineering, *7*(4), 461–471.

Kotov, D. V., Truhlík, V., Richards, P. G., Stankov, S., Bogomaz, O. V., Chernogor, L. F., & Domnin, I. F. (2015). Night-time light ion transition height behaviour over the kharkiv (50 n, 36 e) is radar during the equinoxes of 2006–2010. *Journal of Atmospheric and Solar-Terrestrial Physics*, *132*, 1–12.

Rishbeth, H., & Garriott, O. K. (1969). Introduction to ionospheric physics. *Introduction to ionospheric physics*.

Třísková, L., Truhlík, V., & Šmilauer, J. (2003). An empirical model of ion composition in the outer ionosphere. *Advances in Space Research*, *31*(3), 653–663.

Truhlík, V., Bilitza, D., & Třísková, L. (2015). Towards better description of solar activity variation in the international reference ionosphere topside ion composition model. *Advances in Space Research*, *55*(8), 2099–2105.

Truhlík, V., Třísková, L., & Šmilauer, J. (2004). New advances in empirical modelling of ion composition in the outer ionosphere. *Advances in Space Research*, *33*(6), 844–849.

Vickrey, J. F., Swartz, W. E., & Farley, D. T. (1976). Incoherent scatter measurements of ion counterstreaming. *Geophysical Research Letters*, *3*(4), 217–220.

Vickrey, J. F., Swartz, W. E., & Farley, D. T. (1979a). Ion transport in the topside ionosphere at arecibo. *Journal of Geophysical Research: Space Physics*, *84*(A12), 7307–7314.

Vickrey, J. F., Swartz, W. E., & Farley, D. T. (1979b). Postsunset observations of ionospheric-protonospheric coupling at arecibo. *Journal of Geophysical Research: Space Physics*, *84*(A4), 1310–1314.

West, K., & Heelis, R. (1996). Longitude variations in ion composition in the morning and evening topside equatorial ionosphere near solar minimum. *Journal of Geophysical Research: Space Physics*, *101*(A4), 7951–7960.

Wright, K. H., Swenson, C. M., Thompson, D. C., Barjatya, A., Koontz, S. L., Schneider, T. A., ... others (2008). Charging of the international space station as observed by the floating potential measurement unit: Initial results. *IEEE transactions on plasma science*, *36*(5), 2280–2293. doi: 10.1109/TPS.2008.2003257

Accepted Article

This article is protected by copyright. All rights reserved.

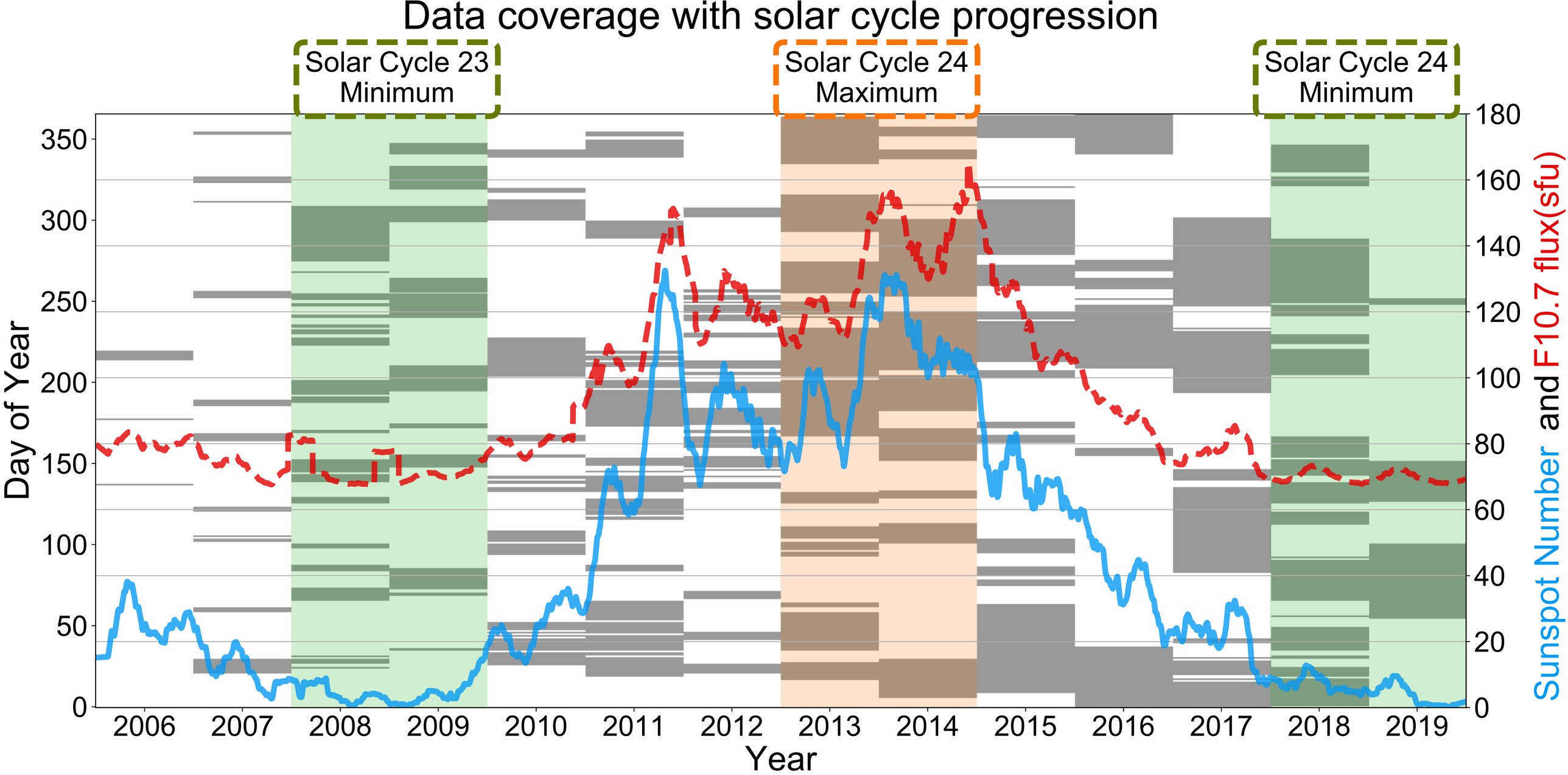
Data coverage with solar cycle progression
Solar Cycle 23 Minimum
Solar Cycle 24 Maximum
Solar Cycle 24 Minimum
Day of Year
Year
Sunspot Number and F10.7 flux(sfu)
0
50
100
150
200
250
300
350
0
20
40
60
80
100
120
140
160
180
2006
2007
2008
2009
2010
2011
2012
2013
2014
2015
2016
2017
2018
2019

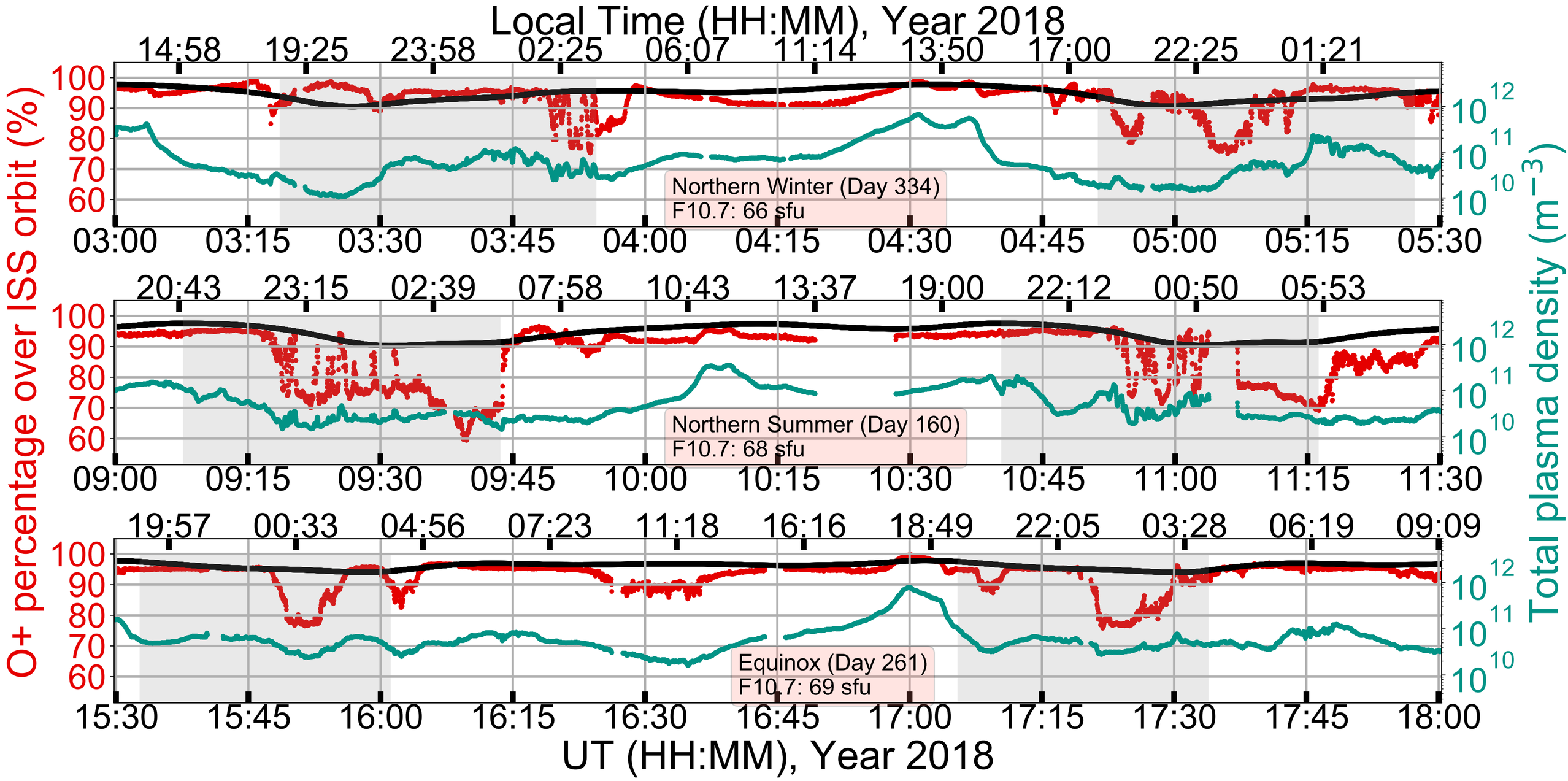
Local Time (HH:MM), Year 2018
14:58
19:25
23:58
02:25
06:07
11:14
13:50
17:00
22:25
01:21
100
90
80
70
60
03:00
03:15
03:30
03:45
04:00
04:15
04:30
04:45
05:00
05:15
05:30
Northern Winter (Day 334)
F10.7: 66 sfu
20:43
23:15
02:39
07:58
10:43
13:37
19:00
22:12
00:50
05:53
09:00
09:15
09:30
09:45
10:00
10:15
10:30
10:45
11:00
11:15
11:30
Northern Summer (Day 160)
F10.7: 68 sfu
19:57
00:33
04:56
07:23
11:18
16:16
18:49
22:05
03:28
06:19
09:09
15:30
15:45
16:00
16:15
16:30
16:45
17:00
17:15
17:30
17:45
18:00
Equinox (Day 261)
F10.7: 69 sfu
O+ percentage over ISS orbit (%)
Total plasma density (m^{-3})
10^{12}
10^{11}
10^{10}
UT (HH:MM), Year 2018

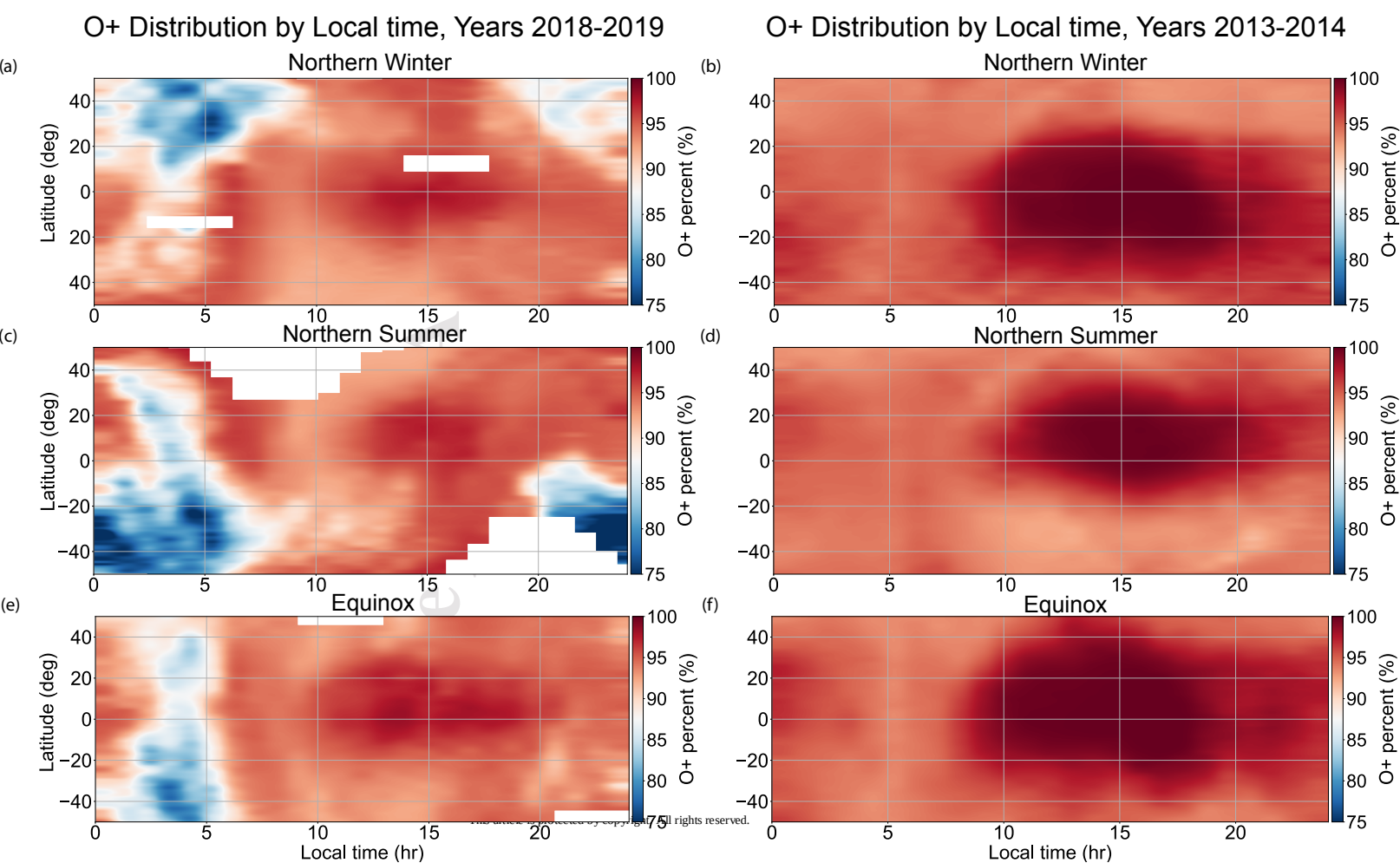
O+ Distribution by Local time, Years 2018-2019
O+ Distribution by Local time, Years 2013-2014
(a)
Northern Winter
(b)
Northern Winter
(c)
Northern Summer
(d)
Northern Summer
(e)
Equinox
(f)
Equinox
Latitude (deg)
O+ percent (%)
Local time (hr)
This article is protected by copyright. All rights reserved.

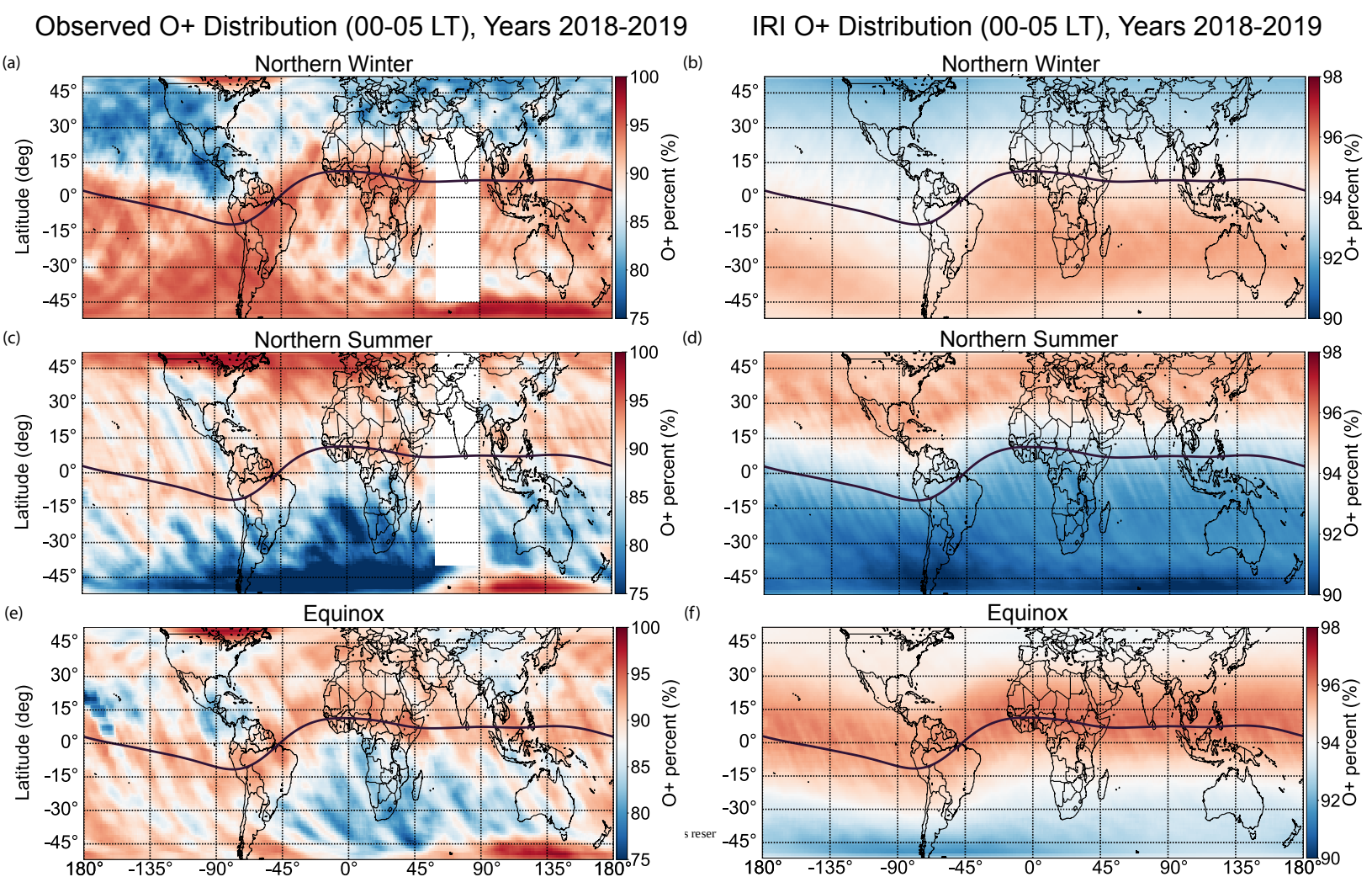
Observed O+ Distribution (00-05 LT), Years 2018-2019
IRI O+ Distribution (00-05 LT), Years 2018-2019
(a)
Northern Winter
(b)
Northern Winter
(c)
Northern Summer
(d)
Northern Summer
(e)
Equinox
(f)
Equinox
Latitude (deg)
O+ percent (%)
45°
30°
15°
0°
-15°
-30°
-45°
100
95
90
85
80
75
98
96
94
92
90
180°
-135°
-90°
-45°
0°
45°
90°
135°
180°

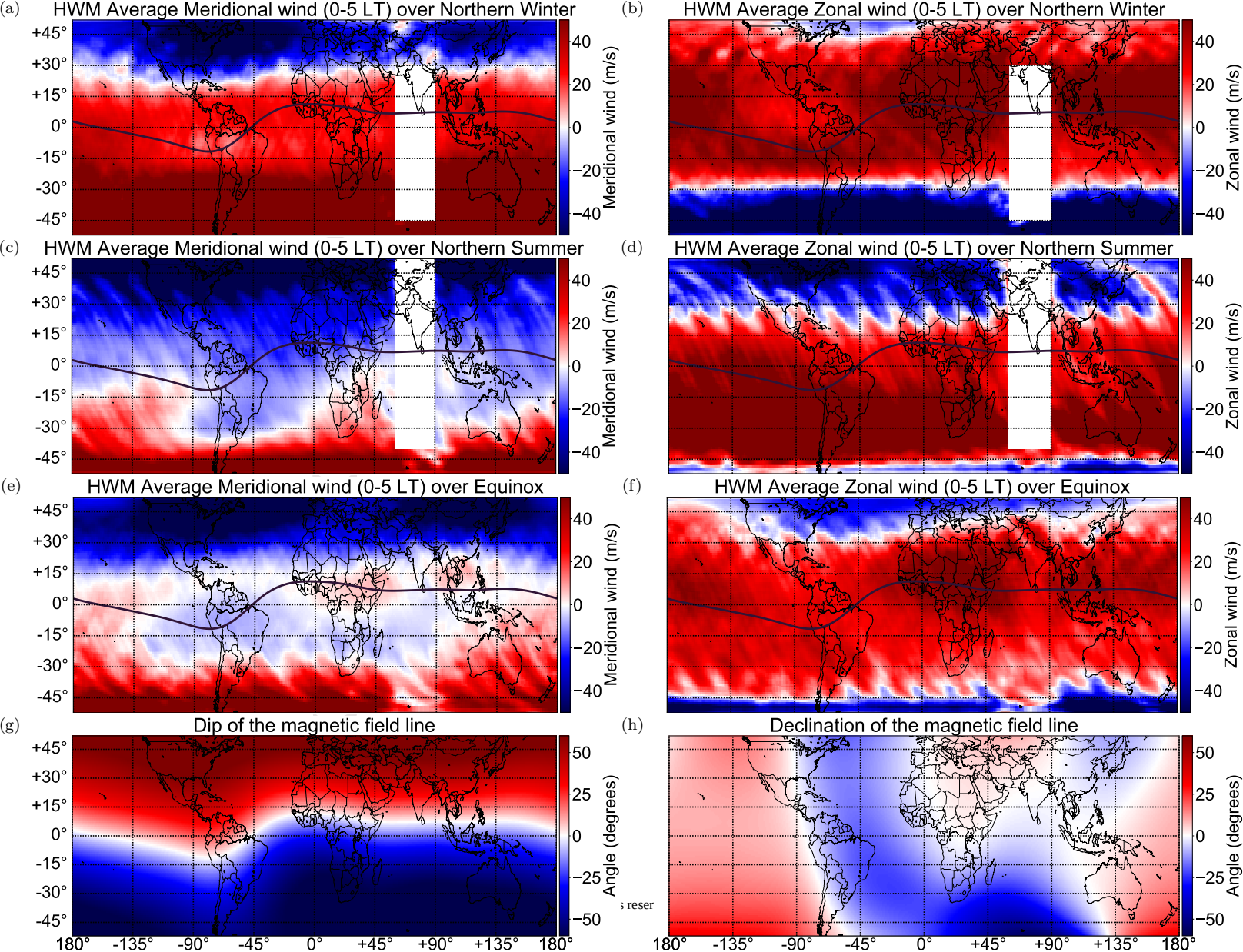
(a)
HWM Average Meridional wind (0-5 LT) over Northern Winter
(b)
HWM Average Zonal wind (0-5 LT) over Northern Winter
(c)
HWM Average Meridional wind (0-5 LT) over Northern Summer
(d)
HWM Average Zonal wind (0-5 LT) over Northern Summer
(e)
HWM Average Meridional wind (0-5 LT) over Equinox
(f)
HWM Average Zonal wind (0-5 LT) over Equinox
(g)
Dip of the magnetic field line
(h)
Declination of the magnetic field line
+45°
+30°
+15°
0°
-15°
-30°
-45°
40
20
0
−20
−40
50
25
−25
−50
Meridional wind (m/s)
Zonal wind (m/s)
Angle (degrees)
180°
-135°
-90°
-45°
0°
+45°
+90°
+135°
180°

s reser